REPORT DOCUMENTATION PAGE

Form Approved
OMB No. 0704-0188

1. REPORT DATE *(DD-MM-YYYY)*	2. REPORT TYPE	3. DATES COVERED *(From - To)*
15-04-2001	Journal Article	2000

4. TITLE AND SUBTITLE
Compensation of charge fluctuations in quantum wells with dual tunneling and photon-assisted escape paths

5a. CONTRACT NUMBER

5b. GRANT NUMBER

5c. PROGRAM ELEMENT NUMBER
62601F

6. AUTHOR(S)
Danhong Huang, Christian Morath, D.A. Cardimona, and Anjali Singh

5d. PROJECT NUMBER
4846

5e. TASK NUMBER
CR

5f. WORK UNIT NUMBER
C1

7. PERFORMING ORGANIZATION NAME(S) AND ADDRESS(ES)

Air Force Research Laboratory
Space Vehicles Directorate
3550 Aberdeen Ave., SE
Kirtland AFB, NM 87117-5776

8. PERFORMING ORGANIZATION REPORT NUMBER

9. SPONSORING / MONITORING AGENCY NAME(S) AND ADDRESS(ES)

10. SPONSOR/MONITOR'S ACRONYM(S)

11. SPONSOR/MONITOR'S REPORT NUMBER(S)

12. DISTRIBUTION / AVAILABILITY STATEMENT
Approved for Public Release; Distribution is Unlimited.

13. SUPPLEMENTARY NOTES
Published in Journal of Applied Physics, Volume 89, Number 8, 15 Apr 2001, pp. 4429 - 4437.

14. ABSTRACT
In our previous article [D. H. Hunang, A. Singh, and D. A. Cardimona, J. Appl. Phys. **87,** 2427 (200)], we explained the experimentally observed zero-bias residual tunneling current [A. Singh and D. A. Cardimona, Opt Eng. **38,** 1424 (1999)] in quantum-well photodetectors biased by an ac voltage. In this article, we extend our theory to include the photoemission current and reproduce our recent finding on the dynamical drop of photoresponsivity $\mathcal{R}_{ph}(t)$ from its static value $\mathcal{R}^0_{ph}$ in quantum-well photodetectors as a function of the chopping frequency of the incident optical flux. In this theory, we derive a dynamical equation for a nonadiabatic space-charge field $\mathcal{E}_{na}(t)$ in the presence of an applied electric field $\mathcal{E}_a(t)$ and an incident optical flux $\Phi_{op}(t)$. From it, a compensation of the charge fluctuations in quantim wells is predicted as a result of dual tunneling and photon-assisted escaping paths. We also find a suppression of the nonadiabatic deviation of $\mathcal{R}_{ph}(t)$ from $\mathcal{R}^0_{ph}$ due to a charge-depletion effect in quantum wells.

15. SUBJECT TERMS
photodectors, quantum wells, nonadiabatic,

16. SECURITY CLASSIFICATION OF:			17. LIMITATION OF ABSTRACT	18. NUMBER OF PAGES	19a. NAME OF RESPONSIBLE PERSON
a. REPORT	b. ABSTRACT	c. THIS PAGE			Mr. David Cardimona
Unclassified	Unclassified	Unclassified	Unlimited	10	19b. TELEPHONE NUMBER *(include area code)* (505) 846-5807

Standard Form 298 (Rev. 8-98)
Prescribed by ANSI Std. 239.18

Compensation of charge fluctuations in quantum wells with dual tunneling and photon-assisted escape paths

Danhong Huang,[a] Anjali Singh,[b] D. A. Cardimona, and Christian Morath
Air Force Research Laboratory (AFRL/VSSS), 3550 Aberdeen Avenue S.E., Building 426, Kirtland Air Force Base, New Mexico 87117

(Received 8 August 2000; accepted for publication 2 January 2001)

In our previous article [D. H. Huang, A. Singh, and D. A. Cardimona, J. Appl. Phys. **87**, 2427 (2000)], we explained the experimentally observed zero-bias residual tunneling current [A. Singh and D. A. Cardimona, Opt. Eng. **38**, 1424 (1999)] in quantum-well photodetectors biased by an ac voltage. In this article, we extend our theory to include the photoemission current and reproduce our recent findings on the dynamical drop of photoresponsivity $\mathcal{R}_{ph}(t)$ from its static value $\mathcal{R}_{ph}^{0}$ in quantum-well photodetectors as a function of the chopping frequency of the incident optical flux. In this theory, we derive a dynamical equation for a nonadiabatic space-charge field $\mathcal{E}_{na}(t)$ in the presence of an applied electric field $\mathcal{E}_b(t)$ and an incident optical flux $\Phi_{op}(t)$. From it, a compensation of the charge fluctuations in quantum wells is predicted as a result of dual tunneling and photon-assisted escaping paths. We also find a suppression of the nonadiabatic deviation of $\mathcal{R}_{ph}(t)$ from $\mathcal{R}_{ph}^{0}$ due to a charge-depletion effect in the quantum wells. © *2001 American Institute of Physics.* [DOI: 10.1063/1.1351867]

I. INTRODUCTION

In two recent articles,[1,2] we found a residual tunneling current in multiple quantum wells when an ac bias voltage sweeps through zero. A circuit model[1] including an important tunneling resistance in series with a quantum-well capacitance was devised to explain this phenomenon,[1] and a satisfactory numerical simulation was obtained by using this phenomenological model. It indicates that a physical process with a very large time constant is involved in transport through multiple quantum wells (MQWs). The microscopic origin of this observation was explored thereafter,[2] and a current instability and hysteresis, as well as a current "arch" and "ripple," were predicted and confirmed experimentally.

It is well known that resonant electron tunneling in MQWs can occur only when the barrier between adjacent quantum wells is thin. If the barrier is very thick, the phase of the wave function will be completely lost as an electron tunnels from one well to another. As a result, only sequential electron tunneling exists for thick barriers. If a dc electric field $\mathcal{E}_b$ is applied to the system, electrons in quantum wells simply respond to it through an adiabatic tunneling current $I_t[\mathcal{E}_b]$ which is a nonlinear function of $\mathcal{E}_b$ due to sequential electron tunneling. We have found that when a time-dependent electric field $\mathcal{E}_b(t)$ is applied to the system, it induces a fluctuation in the charge density inside the quantum wells around the equilibrium value n_{2D}. This gives rise to a nonadiabatic space-charge field $\mathcal{E}_{na}(t)$ which modifies the adiabatic tunneling current $I_t[\mathcal{E}_b(t)]$ by adding a nonadiabatic correction $\Delta I_t(t)$. Under this situation, $\Delta I_t(t)$ remains in-phase with $\mathcal{E}_{na}(t)$, and the dynamics of $\mathcal{E}_{na}(t)$ are determined by the source term $d\mathcal{E}_b(t)/dt$ and the usual quantum-well *charging/discharging* process. If $\mathcal{E}_{na}(t)$ is positive, which shifts the Fermi energy down, the quantum well is discharged with its transient charge density lower than n_{2D}. The quantum well can also be charged when $\mathcal{E}_{na}(t)$ becomes negative.

When one uses a quantum-well photodetector to look for a distant target buried in cold outer space (~4 K), the device temperature must be kept very low (T_e~40 K) in order to minimize the noise and enhance the signal-to-noise ratio. In addition, when the target is moving, a multiple sampling process is required to detect the target motion and reduce the noise by turning the shutter of a photodetector on and off. However, a drop of the photoresponsivity of the device was found[3] when the shutter frequency exceeded a threshold value. This threshold frequency Ω_{th}^{*} depended on the device temperature, the external bias voltage and the incident optical flux. The effect of a shutter can be simulated by a chopped incident optical flux $\Phi_{op}(t)$. When the quantum-well photodetector is exposed to $\Phi_{op}(t)$, the charge density in the quantum wells again fluctuates around n_{2D}. As explained in the tunneling case earlier, a nonadiabatic space-charge field $\mathcal{E}_{na}(t)$ will be induced in the system. Here, the dynamics of $\mathcal{E}_{na}(t)$ are determined by the source term $d\Phi_{op}(t)/dt$ and the usual quantum-well *charging/discharging* process with its decay-time depending on $\Phi_{op}(t)$. Moreover, $\mathcal{E}_{na}(t)$ not only modifies the adiabatic photoemission current $I_e[\mathcal{E}_b,\Phi_{op}(t)]$ by subtracting an out-of-phase correction $\Delta I_e(t)$ relative to $\Phi_{op}(t)$, but also modifies the tunneling current by adding an in-phase correction $\Delta I_t(t)$.

When the charge fluctuates in the quantum wells, the photoresponsivity of the detectors gains a nonadiabatic deviation from the adiabatic value occurring when no charge fluctuation (CF) is present. This will cause a deformation in

[a]Electronic mail: danhong.huang@kirtland.af.mil
[b]Also at: JDS Uniphase Corporation, Monmouth Executive Center, 100 Willowbrook Road, Building 1, Freehold, NJ 07728-2879.

the detected images. We know that the quantum-well CF can be individually controlled by either $d\Phi_{op}(t)/dt$ for a dc electric field or $d\mathcal{E}_b(t)/dt$ with no incident photons. When both a time-dependent electric field $\mathcal{E}_b(t)$ and a time-dependent incident optical flux $\Phi_{op}(t)$ are applied to the system, the CF in the quantum wells will be determined by $d\mathcal{E}_b(t)/dt$ and $d\Phi_{op}(t)/dt$ simultaneously. In this case, both the tunneling and photon-assisted escape channels are open to electron transport. In order to minimize the image deformation, we need to maintain the phase of $\mathcal{E}_b(t)$ opposite to that of $\Phi_{op}(t)$. Under this condition, the CF from these two sources will compensate each other in the quantum wells, and both $\Delta I_t(t)$ and $\Delta I_e(t)$ can be greatly reduced. As a result, the photoresponsivity of the device will approach its adiabatic value and the system will behave close to an ideal adiabatic one.

The organization of this article is as follows. In Sec. II, we present our model beyond the adiabatic limit by deriving a general nonlinear dynamical equation for the nonadiabatic space-charge field in the presence of both a time-dependent electric field and a time-dependent incident optical flux. For the special case with a dc electric field and a time-dependent incident optical flux, the experimentally observed drop of the photoresponsivity as a function of the chopping frequency of the optical flux is reproduced. Numerical results and discussions are given in Sec. III for the nonadiabatic space-charge field, total nonadiabatic photoemission current, and dynamical photoresponsivity when both the electric field and the incident optical flux are time dependent. The article is finally concluded in Sec. IV.

II. MODEL AND THEORY

In this section, we will first study the CF resulting from tunneling transport in the presence of a time-dependent electric field $\mathcal{E}_b(t)$ and no incident photons. Next, the CF resulting from photon-assisted escape will be explored when the only time dependence arises from an incident optical flux $\Phi_{op}(t)$. Finally, the compensation of the CF in quantum wells will be investigated when both $\mathcal{E}_b(t)$ and $\Phi_{op}(t)$ are present.

A. Tunneling

In order to introduce notations and make a comparison between the CFs resulting from either the tunneling or photon-assisted escape, we begin by deriving some of the equations in our previous article.[2]

Let us first consider the tunneling transport of electrons in a MQW system under a bias field $\mathcal{E}_b(t)$. We find that the tunneling current depends not only on $\mathcal{E}_b(t)$ which produces a sequential tunneling current, but also on $d\mathcal{E}_b(t)/dt$.[2] In the nonadiabatic limit, the charge density in each quantum well fluctuates around n_{2D}. It results in a nonadiabatic space-charge field $\mathcal{E}_{na}(t)$ which can be either positive or negative when the charge density in the quantum wells is lower or higher than n_{2D}.

To derive the dynamical equation for $\mathcal{E}_{na}(t)$, we use Levine's sequential electron tunneling model[4] to write down the adiabatic tunneling current $I_t[\mathcal{E}_b(t)]$ under the influence of $\mathcal{E}_b(t)$ in MQWs as

$$I_t[\mathcal{E}_b(t)]=e\mathcal{S}\,v_d[\mathcal{E}_b(t)]n_{\text{eff}}[\mathcal{E}_b(t),T_e], \tag{1}$$

where T_e is the electron temperature (or the device temperature under thermal balance), $\mathcal{S}$ is the sample cross-sectional area, $v_d[\mathcal{E}_b(t)]$ is the electron drift velocity related to $\mathcal{E}_b(t)$ by a saturation model, and $n_{\text{eff}}[\mathcal{E}_b(t),\ T_e]$ is the effective three-dimensional tunneling electron density. In the saturation model, $v_d[\mathcal{E}_b(t)]$ is given by

$$v_d[\mathcal{E}_b(t)]=\frac{v_s}{\sqrt{1+[\mathcal{E}_b(t)/\mathcal{E}_s]^2}}\left[\frac{\mathcal{E}_b(t)}{\mathcal{E}_s}\right], \tag{2}$$

where v_s and $\mathcal{E}_s$ are the saturation velocity and field, respectively. Moreover, we have defined in Eq. (1):

$$n_{\text{eff}}[\mathcal{E}_b(t),T_e]=\left(\frac{m^*}{\pi\hbar^2L_W}\right)\int_0^{+\infty}dE\,T[E,\mathcal{E}_b(t)]\times\left\{f_0\left[\frac{E+E_1-\mu_c(T_e)}{k_BT_e}\right]-f_0\left[\frac{E+E_1+eL_B\mathcal{E}_b(t)-\mu_c(T_e)}{k_BT_e}\right]\right\}, \tag{3}$$

where $f_0(X)$ is the Fermi–Dirac distribution function and $\mu_c(T_e)$ is the chemical potential of electrons in each quantum well. When $\mathcal{E}_b(t)$ is applied, the electrons in the quantum wells will produce a steady-state current flowing in the system. Although the ground-state wave function of the electrons inside the quantum wells can be modified by $\mathcal{E}_b(t)$, the electron density in each well will not change. As a result, $E_1[\mathcal{E}_b(t)]-\mu_c[T_e,\mathcal{E}_b(t)]$ becomes independent of $\mathcal{E}_b(t)$ and thus is simply denoted by $E_1-\mu_c(T_e)$. In Eq. (3), m^* is the effective mass of electrons, L_W is the width of the quantum well, and L_B is the thickness of the barrier between adjacent quantum wells. E_1 is the ground-state energy evaluated at $\mathcal{E}_b(t)=0$, and $\mathcal{T}[E,\mathcal{E}_b(t)]$ is the transmission coefficient of electrons with incident energy E through a barrier biased by $\mathcal{E}_b(t)$. The difference of the Fermi–Dirac distribution functions in Eq. (3) comes from the requirement of an occupied initial state in one well and an unoccupied final state in adjacent well for the sequential tunneling process.

When $d\mathcal{E}_b(t)/dt\neq 0$, there exists a surge tunneling current $I_t^s(t)$ flowing out of the quantum wells in addition to $I_t[\mathcal{E}_b(t)]$.[2] By working in the nonadiabatic limit, $I_t^s(t)$ is given by

$$I_t^s(t)=-e\mathcal{S}\lim_{\Delta t\to 0}\frac{1}{\Delta t}\left\{n_{2D}-\left(\frac{m^*}{\pi\hbar^2}\right)\int_0^{+\infty}dE\times f_0\left[\frac{E+E_1+eL_B\Delta t\ d\mathcal{E}_b(t)/dt-\mu_c(T_e)}{k_BT_e}\right]\right\}$$
$$=-f_0\left[\frac{E_1-\mu_c(T_e)}{k_BT_e}\right]\left(\frac{m^*e^2\mathcal{S}L_B}{\pi\hbar^2}\right)\frac{d\mathcal{E}_b(t)}{dt}. \tag{4}$$

The existence of $I_t^s(t)\propto d\mathcal{E}_b(t)/dt$ causes the imbalance of the tunneling current flowing into and out of a quantum well, which drives the charge density away from n_{2D}. The charge

fluctuation $\Delta Q(t)$ in the quantum wells induces a nonadiabatic space-charge field $\mathcal{E}_{na}(t)$. This gives rise to a nonadiabatic correction to the tunneling current

$$\Delta I_t(t)=e\mathcal{S}\{v_d[\mathcal{E}_b(t)+\mathcal{E}_{na}(t)]\, n_{eff}[\mathcal{E}_b(t)+\mathcal{E}_{na}(t), T_e] - v_d[\mathcal{E}_b(t)]\, n_{eff}[\mathcal{E}_b(t), T_e]\}. \quad (5)$$

In terms of $\mathcal{E}_{na}(t)$, $\Delta Q(t)$ in each quantum well can be expressed as

$$\Delta Q(t)=e\mathcal{S}\left\{n_{2D}-\left(\frac{m^*}{\pi\hbar^2}\right)\times\int_0^{+\infty} dE\, f_0\left[\frac{E+E_1+eL_B\mathcal{E}_{na}(t)-\mu_c(T_e)}{k_BT_e}\right]\right\}. \quad (6)$$

Consequently, the *quantum-mechanical continuity equation* $\Delta I_t(t)+I_t^s(t)+d\Delta Q(t)/dt=0$ leads us to the following dynamical equation for $\mathcal{E}_{na}(t)$:

$$C_{QW}[\mathcal{E}_{na}(t)]\frac{d\mathcal{E}_{na}(t)}{dt} =C_{QW}[0]\frac{d\mathcal{E}_b(t)}{dt}-\left(\frac{e\mathcal{S}}{L_B}\right)\{v_d[\mathcal{E}_b(t)+\mathcal{E}_{na}(t)]n_{eff}[\mathcal{E}_b(t) +\mathcal{E}_{na}(t),T_e]-v_d[\mathcal{E}_b(t)]n_{eff}[\mathcal{E}_b(t),T_e]\}, \quad (7)$$

where $C_{QW}[\mathcal{E}_{na}(t)]$ is the dynamical quantum-well capacitance[5] given by

$$C_{QW}[\mathcal{E}_{na}(t)]=f_0\left[\frac{E_1+eL_B\mathcal{E}_{na}(t)-\mu_c(T_e)}{k_BT_e}\right]\left(\frac{m^*e^2\mathcal{S}}{\pi\hbar^2}\right), \quad (8)$$

which is different from the QW capacitance $C_{QW}[0]$. If $|\mathcal{E}_{na}(t)|\ll|\mathcal{E}_b(t)|$ and $\mu_c(T_e)/eL_B$ for a slowly varying $\mathcal{E}_b(t)$, we can expand Eq. (7) to first order in $\mathcal{E}_{na}(t)$ and arrive at a linear approximation

$$\frac{d\mathcal{E}_{na}(t)}{dt}=\frac{d\mathcal{E}_b(t)}{dt}-\frac{\mathcal{E}_{na}(t)}{R_{tr}[\mathcal{E}_b(t)]C_{QW}[0]}, \quad (9)$$

where $R_{tr}[\mathcal{E}_b(t)]$ is the differential tunneling resistance, given by

$$\frac{1}{R_{tr}[\mathcal{E}_b(t)]}=\left(\frac{e\mathcal{S}}{L_B}\right)\frac{\partial}{\partial\mathcal{E}_b}\{v_d[\mathcal{E}_b(t)]\, n_{eff}[\mathcal{E}_b(t), T_e]\}. \quad (10)$$

Here, T_e is kept constant, and its dependence is not explicitly written out. Equation (9) is a *circuit equation* with respect to $\mathcal{E}_{na}(t)$ in the presence of a source term $d\mathcal{E}_b(t)/dt$, in which $R_{tr}[\mathcal{E}_b(t)]C_{QW}[0]$ plays the role of a *charging/discharging* time constant. This uncovers the microscopic origin of our previous circuit model[1] and explicitly relates the *charging/discharging* time constant to the change of microscopic tunneling current in MQWs.

Using Eq. (9), we have predicted a current hysteresis and a current arch for a sinusoidal $\mathcal{E}_b(t)$, as well as a current ripple for a step-like $\mathcal{E}_b(t)$. A current instability is also found by using Eq. (7). All of these predictions have been confirmed by our previous experiments.[1,2]

B. Photon-assisted escape

In the presence of incident photons, electrons in the ground state can transit to the upper excited state by absorbing photons. From this excited state, they can easily tunnel out to the continuum states above the barrier with help from a dc electric field $\mathcal{E}_b$. Consequently, a photon-assisted escape channel is opened for electrons to get out of quantum wells in addition to the previous tunneling channel.

In the adiabatic limit, by using Levine's electron photoemission model[4], we can write the adiabatic photo-emission current as

$$I_e[\mathcal{E}_b, \Phi_{op}(t)]=e\mathcal{S}\, P_e[\mathcal{E}_b]\sigma_{op}[\omega, \mathcal{E}_b]n_{2D}\Phi_{op}(t), \quad (11)$$

where ω is the frequency of the incident light, $P_e[\mathcal{E}_b]$ is the escape probability of electrons from the upper excited state to the continuum states above the barriers, $\sigma_{op}[\omega, \mathcal{E}_b]$ is the optical cross section which is related to the absorption coefficient by $\sigma_{op}[\omega, \mathcal{E}_b]=\beta_{abs}[\omega, \mathcal{E}_b]L_W/n_{2D}$ in the limit of $\beta_{abs}[\omega, \mathcal{E}_b]L_W\ll 1$, and $\Phi_{op}(t)$ is the incident optical flux. For the escape probability, we use the following empirical formula[4]

$$P_e[\mathcal{E}_b]=\left[1+A_0\exp\left(-\frac{\mathcal{E}_b}{\mathcal{E}_{es}}\right)\right]^{-1}, \quad (12)$$

where A_0 is the zero-field escape time ratio and $\mathcal{E}_{es}$ is the effective barrier lowering field. A more accurate escape probability can be calculated by using the time evolution method.[6] However, the use of Eq. (12) is adequate for elucidating the basic physics for the compensation of CF in quantum wells. For the absorption coefficient, we have[7]

$$\beta_{abs}[\omega, \mathcal{E}_b]=\frac{\sqrt{\epsilon_b}}{n_r[\omega, \mathcal{E}_b]}\left(\frac{\omega}{c}\right)\times[1+\rho_{ph}(\hbar\omega/k_BT_e)]Im\ \alpha_L[\omega,\mathcal{E}_b], \quad (13)$$

where $\rho_{ph}(X)$ is the Bose–Einstein distribution function for photons. In Eq. (13), ϵ_b is the relative dielectric constant of quantum wells,

$$n_r[\omega, \mathcal{E}_b]=[\tfrac{1}{2}+\tfrac{1}{2}\,\mathrm{Re}\ \alpha_L[\omega, \mathcal{E}_b] +\tfrac{1}{2}\sqrt{(1+\mathrm{Re}\ \alpha_L[\omega, \mathcal{E}_b])^2} +\tfrac{1}{2}(\mathrm{Im}\ \alpha_L[\omega, \mathcal{E}_b])^2]^{1/2} \quad (14)$$

is the dynamical refractive index function, and the Lorentz ratio is given by

$$\alpha_L[\omega, \mathcal{E}_b]=-\left(\frac{n_{2D}e^2}{\epsilon_0\epsilon_bL_W}\right)|\langle\xi_1(z)|z|\xi_0(z)\rangle|^2\times\left[\frac{1}{(\hbar\omega-\hbar\Omega_{10}[\mathcal{E}_b])+i\gamma}-\frac{1}{(\hbar\omega+\hbar\Omega_{10}[\mathcal{E}_b])+i\gamma}\right], \quad (15)$$

where $\hbar\Omega_{10}[\mathcal{E}_b]$ is the energy separation between the ground and upper excited states, γ is the homogeneous energy-level broadening, and $|<\xi_1(z)|ez|\xi_0(z)>|^2$ is the square of the transition dipole moment between the ground state $\xi_0(z)$ and

excited state $\xi_1(z)$. Here, $\xi_0(z)$ and $\xi_1(z)$ depend on $\mathcal{E}_b$ due to the Stark effect. In Eq. (15), the Coulomb renormalization of the electron energy levels can be included using the self-consistent Hartree–Fock calculation.[7] The many-body depolarization effect[7] has been neglected. It will shift the absorption peak slightly due to the screening of the Coulomb interaction between electrons.

Because $\Phi_{op}(t)$ varies with time, it induces a CF in the quantum wells in the nonadiabatic limit, once again giving rise to a $\Delta Q(t)$ and a $\Delta I_t(t)$ as given in Eqs. (5) and (6). In this case, however, we have an additional nonadiabatic correction to the photoemission current flowing out of the quantum wells, given by

$$\Delta I_e(t)=e\mathcal{S}\,P_e[\mathcal{E}_b]\sigma_{op}[\omega,\mathcal{E}_b]\,\Phi_{op}(t)\times\left\{n_{2D}-\left(\frac{m^*}{\pi\hbar^2}\right)\int_0^{+\infty}dE\times f_0\left[\frac{E+E_1+eL_B\mathcal{E}_{na}(t)-\mu_c(T_e)}{k_BT_e}\right]\right\}. \tag{16}$$

Here, we have neglected the secondary corrections due to $\mathcal{E}_{na}(t)$ to the escape probability and optical cross section. Moreover, because $d\Phi_{op}(t)/dt\neq 0$, there exists a surge escaping current $I_e^s(t)$ flowing out of quantum wells

$$I_e^s(t)=-e\mathcal{S}\,P_e[\mathcal{E}_b]\sigma_{op}[\omega,\mathcal{E}_b]n_{2D}\,\tau_i\frac{d\Phi_{op}(t)}{dt}, \tag{17}$$

where τ_i is the lifetime of the excited electrons. The existence of $I_e^s(t)\propto d\Phi_{op}(t)/dt$ induces the imbalance between the emission and capture currents flowing out of and into a quantum well, which deviates the charge density away from n_{2D}. The capture probability in Eq. (17) is given by the empirical formula[4]

$$P_c[\mathcal{E}_b]=\left[1+B_\infty\exp\left(-\frac{\mathcal{E}_{cp}}{\mathcal{E}_b}\right)\right]^{-1}, \tag{18}$$

with B_∞ and $\mathcal{E}_{cp}$ being the high-field capture coefficient and effective well capturing field, respectively. Capture probability can be more accurately calculated by adopting the Fermi golden rule method.[8] Applying the *quantum-mechanical continuity equation* $\Delta I_t(t)+\Delta I_e(t)+I_e^s(t)+d\Delta Q(t)/dt=0$, with $\Delta I_t(t)$ and $\Delta Q(t)$ given by Eqs. (5) and (6), leads to the following dynamical equation for $\mathcal{E}_{na}(t)$:

$$\begin{aligned}C_{QW}[\mathcal{E}_{na}(t)]\frac{d\mathcal{E}_{na}(t)}{dt}=&\left(\frac{e\mathcal{S}}{L_B}\right)P_e[\mathcal{E}_b]\sigma_{op}[\omega,\mathcal{E}_b]n_{2D}\,\tau_i\frac{d\Phi_{op}(t)}{dt}\\&-\left(\frac{e\mathcal{S}}{L_B}\right)\{v_d[\mathcal{E}_b+\mathcal{E}_{na}(t)]\,n_{eff}[\mathcal{E}_b+\mathcal{E}_{na}(t),T_e]-v_d[\mathcal{E}_b]\,n_{eff}[\mathcal{E}_b,T_e]\}\\&-\left(\frac{m^*e\mathcal{S}}{\pi\hbar^2L_B}\right)P_e[\mathcal{E}_b]\sigma_{op}[\omega,\mathcal{E}_b]\,\Phi_{op}(t)\\&\times\int_0^{+\infty}dE\left\{f_0\left[\frac{E+E_1-\mu_c(T_e)}{k_BT_e}\right]-f_0\left[\frac{E+E_1+eL_B\mathcal{E}_{na}(t)-\mu_c(T_e)}{k_BT_e}\right]\right\}.\end{aligned} \tag{19}$$

In the limit of $|\mathcal{E}_{na}(t)|\ll|\mathcal{E}_b|$ and $\mu_c(T_e)/eL_B$ for a slowly varying $\Phi_{op}(t)$, we can expand Eq. (19) to first order in $\mathcal{E}_{na}(t)$ and arrive at a linear equation

$$C_{QW}[0]\frac{d\mathcal{E}_{na}(t)}{dt}=\left(\frac{e\mathcal{S}\tau_{op}[\mathcal{E}_b]}{L_B}\right)\frac{d\Phi_{op}(t)}{dt}-\mathcal{E}_{na}(t)\left\{\frac{1}{R_{tr}[\mathcal{E}_b]}+\frac{1}{R_{op}[\mathcal{E}_b,\Phi_{op}(t)]}\right\}, \tag{20}$$

where the optoresistance and phototraverse time are defined, respectively, by

$$\frac{1}{R_{op}[\mathcal{E}_b,\Phi_{op}(t)]}=P_e[\mathcal{E}_b]\sigma_{op}[\omega,\mathcal{E}_b]\,\Phi_{op}(t)\,C_{QW}[0], \tag{21}$$

$$\tau_{op}[\mathcal{E}_b]=\tau_i\,P_e[\mathcal{E}_b]\sigma_{op}[\omega,\mathcal{E}_b]n_{2D}. \tag{22}$$

In Eq. (21), $1/R_{op}[\mathcal{E}_b,\Phi_{op}(t)]$ describes how easy one electron can transit from the ground state to the upper excited state and then escape out to the continuum state above the barrier. By comparing Eq. (20) with Eq. (9), we get the effective resistance $1/R_{eff}[\mathcal{E}_b,\Phi_{op}(t)]=1/R_{tr}[\mathcal{E}_b]+1/R_{op}[\mathcal{E}_b,\Phi_{op}(t)]$ in the *circuit equation* for the dual tunneling and photon-assisted escape channels, the source term $(e\mathcal{S}\tau_{op}[\mathcal{E}_b]/L_BC_{QW}[0])d\Phi_{op}(t)/dt$, and the *charging/discharging* time constant $R_{eff}[\mathcal{E}_b,\Phi_{op}(t)]C_{QW}[0]$.

C. Compensation of charge fluctuations

In the presence of both $\mathcal{E}_b(t)$ and $\Phi_{op}(t)$, from the *quantum-mechanical continuity equation* $\Delta I_t(t)+I_t^s(t)+\Delta I_e(t)+I_e^s(t)+d\Delta Q(t)/dt=0$ we get the dynamical equation for $\mathcal{E}_{na}(t)$ by combining Eqs. (7) and (19):

$$C_{QW}[\mathcal{E}_{na}(t)]\frac{d\mathcal{E}_{na}(t)}{dt}=C_{QW}[0]\frac{d\mathcal{E}_b(t)}{dt}+\left(\frac{e\mathcal{S}\tau_{op}[\mathcal{E}_b(t)]}{L_B}\right)\frac{d\Phi_{op}(t)}{dt}$$
$$-\left(\frac{e\mathcal{S}}{L_B}\right)\{v_d[\mathcal{E}_b(t)+\mathcal{E}_{na}(t)]\,n_{eff}[\mathcal{E}_b(t)+\mathcal{E}_{na}(t),T_e]-v_d[\mathcal{E}_b(t)]\,n_{eff}[\mathcal{E}_b(t),T_e]\}$$
$$-\left(\frac{m^*e\mathcal{S}}{\pi\hbar^2L_B}\right)\left\{\frac{1}{R_{op}[\mathcal{E}_b(t),\Phi_{op}(t)]C_{QW}[0]}\right\}$$
$$\times\int_0^{+\infty}dE\left\{f_0\left[\frac{E+E_1-\mu_c(T_e)}{k_BT_e}\right]-f_0\left[\frac{E+E_1+eL_B\mathcal{E}_{na}(t)-\mu_c(T_e)}{k_BT_e}\right]\right\}. \tag{23}$$

In the limit of slowly varying $\mathcal{E}_b(t)$ and $\Phi_{op}(t)$, by combining Eqs. (9) and (20) we are led to the linear approximation of Eq. (23):

$$C_{QW}[0]\frac{d\mathcal{E}_{na}(t)}{dt}$$
$$=C_{QW}[0]\frac{d\mathcal{E}_b(t)}{dt}+\left\{\frac{e\mathcal{S}\tau_{op}[\mathcal{E}_b(t)]}{L_B}\right\}\frac{d\Phi_{op}(t)}{dt}$$
$$-\mathcal{E}_{na}(t)\left\{\frac{1}{R_{tr}[\mathcal{E}_b(t)]}+\frac{1}{R_{op}[\mathcal{E}_b(t),\Phi_{op}(t)]}\right\}. \tag{24}$$

The individual source terms $d\mathcal{E}_b(t)/dt$ and $\{e\mathcal{S}\tau_{op}[\mathcal{E}_b(t)]/L_BC_{QW}[0]\}d\Phi_{op}(t)/dt$ in Eq. (24) can be either in-phase or out-of-phase with each other. When they are in-phase, the effects of the CF from these two channels become constructive. When they are out-of-phase, the effects are destructive. This gives rise to a compensation of the CF in quantum wells from dual tunneling and photon-assisted escape channels.

Since the general nonlinear Eqs. (7) and (19) and their linear approximations in Eqs. (9) and (20) are all confirmed by our experiments, the validity of Eq. (23) by combining Eqs. (7) and (19) or its linear approximation in Eq. (24) by combing Eqs. (9) and (20) is guaranteed. Therefore, we believe that the prediction made from Eqs. (23) and (24) in our numerical results later for the compensation of the CF in quantum wells should be observable in a future experiment.

D. Photoresponsivity

The *dynamical* photoresponsivity of the system in the presence of $\mathcal{E}_b(t)$ and $\Phi_{op}(t)$ is defined by the photoemission current with transient charge density at time t in each quantum well[4] and is given by

$$\mathcal{R}_{ph}(t)=\frac{I_e[\mathcal{E}_b(t),\Phi_{op}(t)]-\Delta I_e(t)}{\hbar\omega P_c[\mathcal{E}_b(t)]\mathcal{S}\Phi_{op}(t)}. \tag{25}$$

In the special case of $d\mathcal{E}_b(t)/dt=0$ and a slowly varying $\Phi_{op}(t)$, we find from Eq. (25)

$$\mathcal{R}_{ph}(t)=\mathcal{R}^0_{ph}\left\{1-\left(\frac{L_B}{eP_e[\mathcal{E}_b]\sigma_{op}[\omega,\mathcal{E}_b]n_{2D}\,\Phi_{op}(t)\mathcal{S}}\right\}\right.$$
$$\left.\times\left(\frac{1}{R_{op}[\mathcal{E}_b,\Phi_{op}(t)]}\right)\mathcal{E}_{na}(t)\right\}, \tag{26}$$

where the static photoresponsivity is

$$\mathcal{R}^0_{ph}=\frac{eP_e[\mathcal{E}_b]\sigma_{op}[\omega,\mathcal{E}_b]n_{2D}}{\hbar\omega P_c[\mathcal{E}_b]}. \tag{27}$$

By assuming an optical flux $\Phi_{op}(t)=\Phi_0+\Phi_m\exp(i\Omega_ct)$, where Ω_c and Φ_m are the frequency and modulation amplitude of $\Phi_{op}(t)$ and Φ_0 is the background optical flux, we take the Fourier transform of Eq. (20) in the limit of weak modulation $\Phi_m/\Phi_0\ll1$ and get the leading term of $\mathcal{E}_{na}(\bar{\Omega}_F)$:

$$\mathcal{E}_{na}(\bar{\Omega}_F)=i\frac{e\mathcal{S}\tau_{op}[\mathcal{E}_b]\Omega_c\Phi_mR^*[\mathcal{E}_b]\delta(\bar{\Omega}_F-\Omega_c)}{L_B(1+i\bar{\Omega}_FR^*[\mathcal{E}_b]C_{QW}[0])}$$
$$-i\left(\frac{R^*[\mathcal{E}_b]}{R^0_{op}[\mathcal{E}_b]}\right)\left(\frac{\Phi_m}{\Phi_0}\right)\frac{e\mathcal{S}\tau_{op}[\mathcal{E}_b]\Omega_c\Phi_mR^*[\mathcal{E}_b]\delta(\bar{\Omega}_F-2\Omega_c)}{L_B(1+i\bar{\Omega}_FR^*[\mathcal{E}_b]C_{QW}[0])\{1+i(\bar{\Omega}_F-\Omega_c)R^*[\mathcal{E}_b]C_{QW}[0]\}}. \tag{28}$$

Here, $1/R^*[\mathcal{E}_b]=1/R_{tr}[\mathcal{E}_b]+1/R^0_{op}[\mathcal{E}_b]$ with $1/R^0_{op}[\mathcal{E}_b]=P_e[\mathcal{E}_b]\sigma_{op}[\omega,\mathcal{E}_b]\,\Phi_0C_{QW}[0]$. Moreover, we take the Fourier transform of Eq. (26) and get

$$\mathcal{R}_{ph}(\bar{\Omega}_F)=\mathcal{R}^0_{ph}\left\{\delta(\bar{\Omega}_F)-\frac{L_BC_{QW}[0]}{en_{2D}\mathcal{S}}\mathcal{E}_{na}(\bar{\Omega}_F)\right\}. \tag{29}$$

From Eqs. (28) and (29), we find the drop of the photoresponsivity to be

$$\Delta\mathcal{R}_{\rm ph}(\Omega_c)=\left|\mathcal{R}^0_{\rm ph}-\int_{-\infty}^{+\infty}d\bar{\Omega}_F\,\mathcal{R}_{\rm ph}(\bar{\Omega}_F)\right|=\mathcal{R}^0_{ph}\left(\frac{L_B C_{\rm QW}[0]}{en_{\rm 2D}\mathcal{S}}\right)\left|\int_{-\infty}^{+\infty}d\bar{\Omega}_F\,\mathcal{E}_{\rm na}(\bar{\Omega}_F)\right|$$

$$=\mathcal{R}^0_{\rm ph}\left(\frac{\Phi_m\tau_{\rm op}[\mathcal{E}_b]}{n_{\rm 2D}}\right)\left[\frac{\Omega_c}{\sqrt{1/(R^*[\mathcal{E}_b]C_{\rm QW}[0])^2+\Omega_c^2}}\right]$$

$$\times\left\{\sqrt{\frac{[1-(R^*[\mathcal{E}_b]/R^0_{\rm op}[\mathcal{E}_b])(\Phi_m/\Phi_0)]^2+4(R^*[\mathcal{E}_b]C_{\rm QW}[0])^2\Omega_c^2}{1+4(R^*[\mathcal{E}_b]C_{\rm QW}[0])^2\Omega_c^2}}\right\}, \tag{30}$$

which is zero for $\Omega_c=0$ and $\mathcal{R}^0_{\rm ph}(\Phi_m\tau_{\rm op}[\mathcal{E}_b]/n_{\rm 2D})$ for $\Omega_c \gg 1/(R^*[\mathcal{E}_b]C_{\rm QW}[0])$. The chopping frequency at which the photoresponsivity has dropped halfway between the maximum and minimum values is found to be

$$\Omega^*_{\rm th}=1/(R^*[\mathcal{E}_b]C_{\rm QW}[0])\ . \tag{31}$$

Figure 1 is taken from an early measurement performed by Arrington, *et al.*[3] and shows the quantum efficiency-gain product in (a) as a function of Ω_c and the extracted $\Omega^*_{\rm th}$ in (b). In Fig. 1(a), the dynamical suppression of the photoresponsivity is clearly seen as a function of Ω_c for various average incident photon irradiances $\bar{\Phi}=\sqrt{\langle[\Phi_{\rm op}(t)]^2\rangle}$. In Fig. 1(b), $\Omega^*_{\rm th}$ is plotted as a function of $\bar{\Phi}$ at $T=40$ *K* for different dc bias voltages V_b. For $V_b=-1.5$ V, $\Omega^*_{\rm th}$ appears as a linear function of $\bar{\Phi}$. When V_b is increased to -3.5 V, we find $\Omega^*_{\rm th}$ is a linear function of Φ only when Φ is large but becomes independent of $\bar{\Phi}$ when $\bar{\Phi}$ is small. We know that at low biases, $R_{\rm tr}[\mathcal{E}_b]\gg R^0_{\rm op}[\mathcal{E}_b]$ and $1/R^*[\mathcal{E}_b]\approx 1/R^0_{\rm op}[\mathcal{E}_b]$ where $R^0_{\rm op}[\mathcal{E}_b]$ is proportional to $\bar{\Phi}$. This leads to $\Omega^*_{\rm th}\propto\bar{\Phi}$ shown in Fig. 1(b) as predicted by Eq. (31). At high biases, the situation is less straightforward. When $\bar{\Phi}$ is small, we find that $R_{\rm tr}[\mathcal{E}_b]\ll R^0_{\rm op}[\mathcal{E}_b]$ and $\Omega^*_{\rm th}$ is independent of $\bar{\Phi}$. At higher flux, $R_{\rm tr}[\mathcal{E}_b]\gg R^0_{\rm op}[\mathcal{E}_b]$ and $\Omega^*_{\rm th}$ is again linearly dependent on $\bar{\Phi}$. Consequently, Eq. (31) is verified experimentally, which proves the validity of Eqs. (19) and (20), as well as the dynamical photoresponsivity $\mathcal{R}_{\rm ph}(t)$ defined in Eq. (25).

In order to further verify the relationship in Eq. (32) beyond the limitation of $\Phi_m/\Phi_0\ll 1$, we present in Fig. 2 the numerical results for $\Delta\mathcal{R}_{\rm ph}(\Omega_c)/\mathcal{R}^0_{\rm ph}$ with $\Phi_m/\Phi_0=1$ and various optical fluxes, device temperatures and bias voltages. From the solid curve, we find a rolling-off feature of $\Delta\mathcal{R}_{\rm ph}(\Omega_c)/\mathcal{R}^0_{\rm ph}$ at $\Omega^*_{\rm th}=0.3$ Hz. As Φ_m decreases from 5×10^{12} cm^{-2} s^{-1} to 1×10^{12} cm^{-2} s^{-1} (dashed curve), the rolling-off point is shifted down because $1/R^*[\mathcal{E}_b]\sim 1/R^0_{\rm op}[\mathcal{E}_b]$ is reduced as predicted by Eq. (32). When T_e increases from 40 to 50 K (dash-dotted curve), $\Omega^*_{\rm th}$ is shifted up because $1/R^*[\mathcal{E}_b]\sim 1/R_{\rm tr}[\mathcal{E}_b]$ increases with T_e rapidly as seen from Eq. (32). Finally, when we reduce $\mathcal{E}_b$ from 25 to 5 kV/cm (dash-dot-dotted curve), we find a down-shift of $\Omega^*_{\rm th}$ since $1/R^*[\mathcal{E}_b]\sim 1/R_{\rm tr}[\mathcal{E}_b]$ decreases with $\mathcal{E}_b$ as implied by Eq. (32). All of these features found in our calculations are consistent with the experimental observations in Figs. 1(a) and 1(b).

III. NUMERICAL RESULTS AND COMPARISONS

In this section, we will present some numerical results to demonstrate the compensation of CF in quantum wells in the

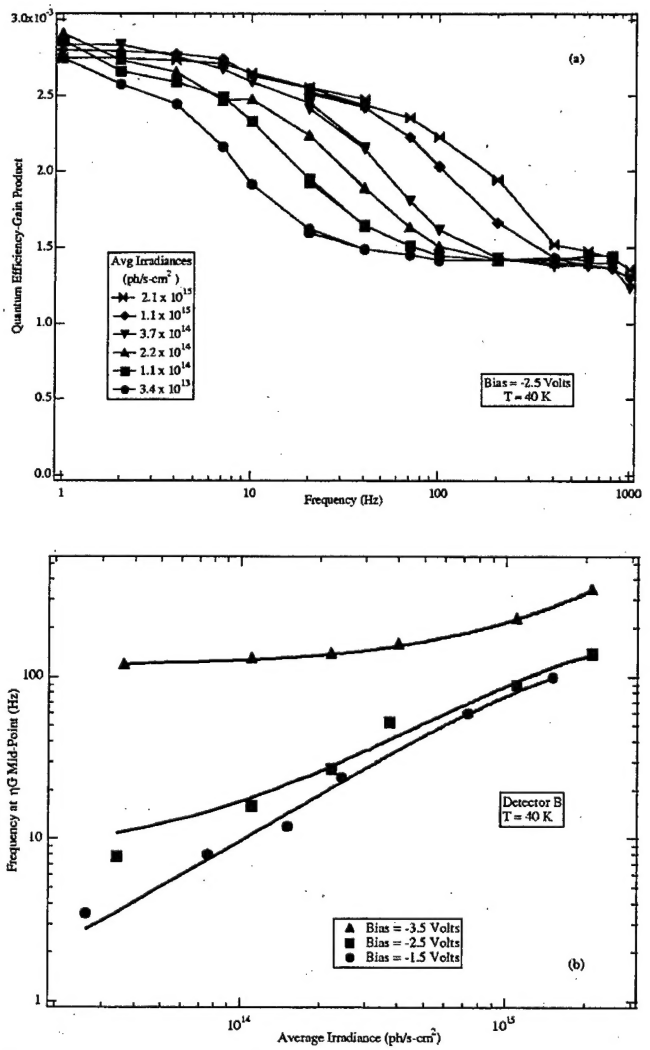

FIG. 1. Measured quantum efficiency-gain product of a sample (see Ref. 3) at $T_e=40$ K and central wavelength $\lambda_0=7.1$ μm as a function of the chopping frequency Ω_c in (a) for different average photon irradiances $\bar{\Phi}$, and the extracted chopping frequency $\Omega^*_{\rm th}$ at which the quantum efficiency-gain product reaches halfway between the maximum and minimum values as a function of $\bar{\Phi}$ in (b) for different bias voltages V_b. In (a), V_b is fixed at -2.5 V and $\bar{\Phi}$ is varied between 3.4×10^{13} and 2.1×10^{15} ph/s cm^2. In (b), the halfway chopping frequency with three various bias voltages $V_b=-1.5$, -2.5, and -3.5 V are displayed as a function of $\bar{\Phi}$.

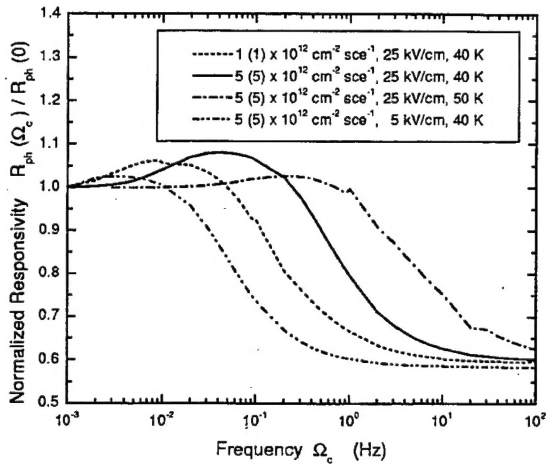

FIG. 2. Comparison of the average photoresponsivity $\sqrt{\langle[\mathcal{R}_{ph}(\bar{\Omega}_F)]^2\rangle}/\mathcal{R}^0_{ph}$ as a function chopping frequency Ω_c for various optical fluxes, device temperatures and bias voltages. Here, we set $\Phi_m/\Phi_0=1$ in our calculation. The solid curve corresponds to $\Phi_m=5\times10^{12}$ cm^{-2} s^{-1}, $\mathcal{E}_b=25$ kV/cm and $T_e=40$ K; the dashed curve to $\Phi_m=1\times10^{12}$ cm^{-2} s^{-1} but the same $\mathcal{E}_b$ and T_e; the dash-dotted curve to $T_e=50$ K but the same Φ_m and $\mathcal{E}_b$; and the dash-dot-dotted curve to $\mathcal{E}_b=5$ kV/cm but the same Φ_m and T_e. Other parameters have been given in Tables I–III.

presence of both $\mathcal{E}_b(t)$ and $\Phi_{op}(t)$. The nonlinear effect beyond the linear model will be considered thereafter.

In our numerical calculation, we have assigned the following forms to $\mathcal{E}_b(t)$ and $\Phi_{op}(t)$:

$$\mathcal{E}_b(t) = \begin{cases} \mathcal{E}_0+\mathcal{E}_m \sin[(2\pi t/T_p)+\alpha_0], & jT_p\leq t\leq(j+1/2)T_p \\ 0, \quad \text{others} \end{cases} \tag{32}$$

for $j=0, 1, 2, \ldots$ and

$$\Phi_{op}(t) = \begin{cases} \Phi_0+\Phi_m \sin[2\pi t/T_p], & jT_p\leq t\leq(j+1/2)T_p \\ 0, \quad \text{others} \end{cases} \tag{33}$$

where α_0 is the phase difference between $\mathcal{E}_b(t)$ and $\Phi_{op}(t)$ and $T_p=2\pi/\Omega_c$ is the time period for both $\mathcal{E}_b(t)$ and $\Phi_{op}(t)$. $\mathcal{E}_0$ and $\mathcal{E}_m$ are the dc component and the amplitude of the ac component of $\mathcal{E}_b(t)$. Φ_0 and Φ_m are the background flux and the amplitude of the modulation component of $\Phi_{op}(t)$. Here, we take $\tau_i=1$ ps. The other sample parameters used in our calculation are listed in Tables I–III, where the photon energy is in resonance with the energy separation between the ground and excited states of a QW.

A. Compensation of charge fluctuations

In this part, we present the numerical results in Figs. 3–5 from the linear model in Eq. (24).

TABLE I. List of internal parameters for GaAs/$Al_{0.3}Ga_{0.7}$As MQWs.

L_W (Å)	L_B (Å)	n_{2D} (10^{11} cm^{-2})	$\mathcal{S}$ (10^{-4} cm^{-2})	v_s (10^6 cm/s)	$\mathcal{E}_s$ (kV/cm)	γ (meV)
50	500	8	2.25	2	2	1

TABLE II. List of external parameters.

$\hbar\omega$ (meV)	$\mathcal{E}_0$ (kV/cm)	α_0	Φ_0, Φ_m (10^{11} cm^{-2})	T_p (s)	T_e (K)
168	25	π	5	400	40

Figure 3 presents the numerical solutions of Eq. (24) for $\mathcal{E}_{na}(t)$ as a function of time t for different values of $\mathcal{E}_m$, the ac component amplitude. When $\mathcal{E}_m=0$ (dash-dot-dotted curve), due to CF in the quantum wells, the induced nonadiabatic space-charge field $\mathcal{E}_{na}(t)$ is driven by $d\Phi_{op}(t)/dt$ over the first half period. This is followed by a decay in the second half-period when $\Phi_{op}(t)=\Phi_0$. The deviation of $\mathcal{E}_{na}(t)$ from zero measures the effect of the CF, which is gradually reduced with the increase of $\mathcal{E}_m$ from zero. Because the phase difference $\alpha_0=\pi$, $\mathcal{E}_b(t)$ and $\Phi_{op}(t)$ are completely out-of-phase with each other and the effects of the CF from the dual tunneling and photon-assisted escape are compensated, leading to a decrease of the deviation of $\mathcal{E}_{na}(t)$ from zero.

We show in Fig. 4 the total nonadiabatic photoemission currents $I_e[\mathcal{E}_b(t), \Phi_{op}(t)]-\Delta I_e(t)$ as a function of time t for different values of $\mathcal{E}_m$. Within the adiabatic limit with $\mathcal{E}_m=0$ (dotted curve), the photoemission current is simply $I_e[\mathcal{E}_0, \Phi_{op}(t)]$, and it is proportional to $\Phi_{op}(t)$. Beyond the adiabatic limit, the total nonadiabatic photoemission current is dramatically reduced compared to the adiabatic value in the first half period, but is enhanced in the second half period. This is due to the fact that $I_e[\mathcal{E}_b(t),\Phi_{op}(t)]-\Delta I_e(t)$ always remains out-of-phase with $d\Phi_{op}(t)/dt$. When an out-of-phase electric field $\mathcal{E}_b(t)$ is applied to the system, $\Delta I_e(t)$ which results from CF in the quantum wells in both the first and second half periods, becomes smaller with increasing $\mathcal{E}_m$. We attribute this to the cancellation of CF in the quantum wells from the dual tunneling and photon-assisted escape paths.

The results of the dynamical photoresponsivity $\mathcal{R}_{ph}(t)$ from Eq. (25) as a function of t for different values of $\mathcal{E}_m$ are compared in Fig. 5. In the adiabatic case with $\mathcal{E}_m=0$, $\mathcal{R}_{ph}(t)$ (dotted line) equals its static value $\mathcal{R}^0_{ph}$, and is independent of $\Phi_{op}(t)$. In the nonadiabatic case, $\mathcal{R}_{ph}(t)$ dramatically decreases compared to $\mathcal{R}^0_{ph}$ in the first half period, but increases in the second half period. In the first period where $\mathcal{E}_{na}(t)>0$, the total nonadiabatic photoemission current is reduced compared to its adiabatic value as shown in Fig. 4. However, $\mathcal{E}_{na}(t)$ switches its sign in the second half period as shown in Fig. 3, which increases the photoemission current. These two factors together give rise to the features of $\mathcal{R}_{ph}(t)$ seen in Fig. 5. When an out-of-phase electric field $\mathcal{E}_b(t)$ is applied to the system, $\mathcal{R}_{ph}(t)$ gradually approaches $\mathcal{R}^0_{ph}$ with the increase of $\mathcal{E}_m$ due to the compensation of the CF. We have noted that the dynamical change of $\mathcal{R}_{ph}(t)$ at $\mathcal{E}_b(t)$

TABLE III. List of emission and capture parameters.

$\mathcal{E}_{es}$ (kV/cm)	A_0	$\mathcal{E}_{cp}$ (kV/cm)	B_∞
4.73	36	2.67	11.5

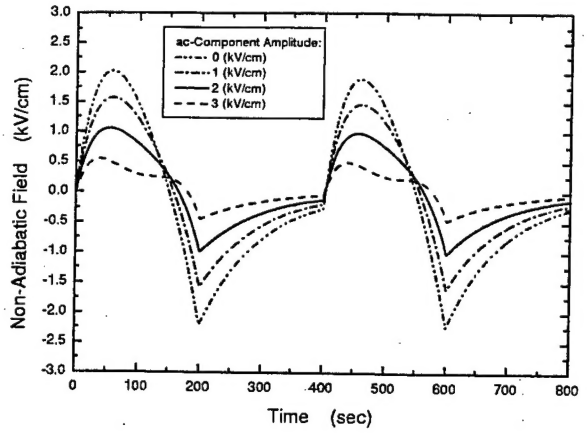

FIG. 3. Nonadiabatic space-charge field $\mathcal{E}_{na}(t)$ as a function of time for different ac-component amplitudes $\mathcal{E}_m=0$, 1, 2, and 3 kV/cm.

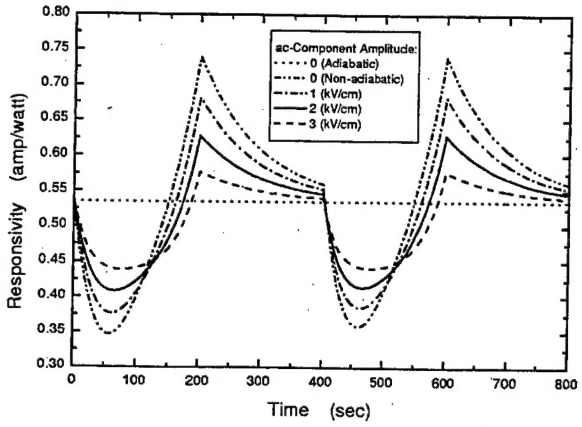

FIG. 5. Dynamical photoresponsivity $\mathcal{R}_{ph}(t)$ as a function of time for different ac-component amplitudes $\mathcal{E}_m=0$, 1, 2, and 3 kV/cm. The static photoresponsivity $\mathcal{R}^0_{ph}$ with $\mathcal{E}_m=0$ (dotted curve) is also included in the figure for the sake of convenience.

$=\mathcal{E}_0$ reaches approximately as high as 40% of its adiabatic value $\mathcal{R}^0_{ph}$. However, this dynamical change is greatly suppressed by the nonlinearity as discussed next.

B. Effect beyond linear model

In this part, we present the numerical results in Figs. 6–9 which compare the linear model in Eq. (20) with the nonlinear model in Eq. (19) at $\mathcal{E}_b(t)=\mathcal{E}_0$.

Figure 6 compares the calculated total electric field $\mathcal{E}_0+\mathcal{E}_{na}(t)$ as a function of t from both the nonlinear model in Eq. (19) and linear model in Eq. (20). In the adiabatic limit, the total electric field (dash-dot-dotted line) is simply $\mathcal{E}_0$. The linear model introduces a large CF in the quantum wells, which enhances $\mathcal{E}_{na}(t)$ in the system. The nonlinearity greatly suppresses the CF (solid curve) resulting from $d\Phi_{op}(t)/dt\neq 0$, giving rise to only a small deviation of the total electric field from $\mathcal{E}_0$. We know that the positive $\mathcal{E}_{na}(t)$ indicates the shift down of the Fermi energy E_f which results from charge depletion in the quantum wells. This will reduce the dynamical QW capacitance $C_{QW}[\mathcal{E}_{na}(t)]$ compared with $C_{QW}[0]$ at finite temperatures but not at $T_e=0\,K$ if $eL_B\mathcal{E}_{na}(t)<E_f-E_1$. From this figure, we see that the discharging process $[d\mathcal{E}_{na}(t)/dt>0]$ is accelerated in the nonlinear model due to $C_{QW}[\mathcal{E}_{na}(t)]<C_{QW}[0]$ in Eq. (8), which produces a small discharging constant in Eq. (19).

The normalized ratio of the CF in quantum wells, $1-[\Delta Q(t)/e\mathcal{S}n_{2D}]$, with $\mathcal{E}_b(t)=\mathcal{E}_0$ using the nonlinear model is presented in Fig. 7. The whole fluctuation process within a period can be described in three successive steps (see Fig. 6): (1) the initial discharging process $d\mathcal{E}_{na}(t)/dt>0$, (2) the intermediate charging process $d\mathcal{E}_{na}(t)/dt<0$, and (3) the final discharging process $d\mathcal{E}_{na}(t)/dt>0$. The maximum "charge depletion" in quantum wells is about 10% of n_{2D} in the initial discharging process and the maximum "charge accumulation" is 15% of n_{2D} at the end of the intermediate charging process.

Because the dynamical photoresponsivity $\mathcal{R}_{ph}(t)$ only depends on the total nonadiabatic photoemission current, we show in Fig. 8 the results of the calculated $I_e[\mathcal{E}_b,\Phi_{op}(t)]-\Delta I_e(t)$ as a function of t with $\mathcal{E}_b(t)=\mathcal{E}_0$ using both the nonlinear model in Eq. (19) and the linear model in Eq. (20). In the adiabatic case, the photoemission current $I_e[\mathcal{E}_0,\Phi_{op}(t)]$ (dash-dot-dotted curve) is proportional to $\Phi_{op}(t)$. Although the CF in the quantum wells induces a

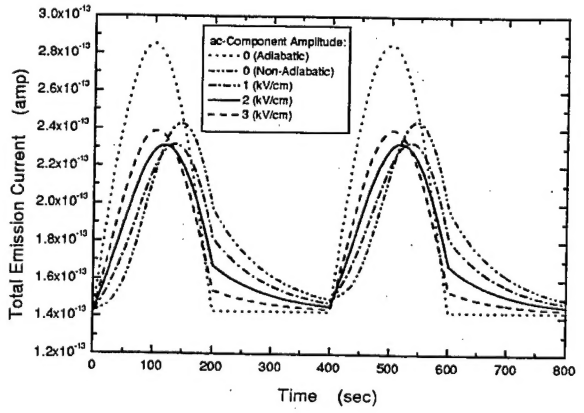

FIG. 4. Total nonadiabatic photoemission current $I_e[\mathcal{E}_b(t),\Phi_{op}(t)]-\Delta I_e(t)$ as a function of time for different ac-component amplitudes $\mathcal{E}_m=0$, 1, 2, and 3 kV/cm. For convenience, the adiabatic photoemission current $I_e[\mathcal{E}_0,\Phi_{op}(t)]$ with $\mathcal{E}_m=0$ (dotted curve) is also included in the figure.

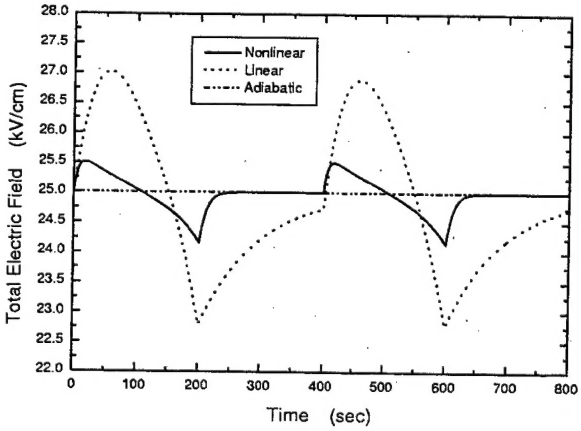

FIG. 6. Total nonadiabatic electric fields $\mathcal{E}_0+\mathcal{E}_{na}(t)$ as a function of time from the nonlinear model in Eq. (19) and linear model in Eq. (20), respectively. The dc electric field $\mathcal{E}_0$ (dash-dot-dotted line) is also included in the figure as a comparison.

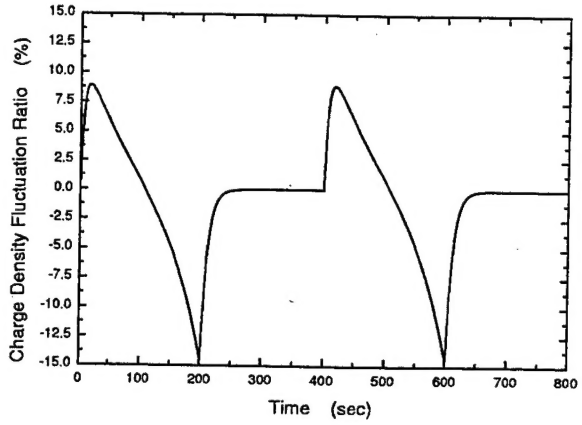

FIG. 7. Normalized ratio of charge fluctuation $[1-\Delta Q(t)/e\mathcal{S}n_{2D}]$ calculated from Eq. (6) using the nonlinear model in Eq. (19) as a function of time for $\mathcal{E}_b(t)=\mathcal{E}_0$.

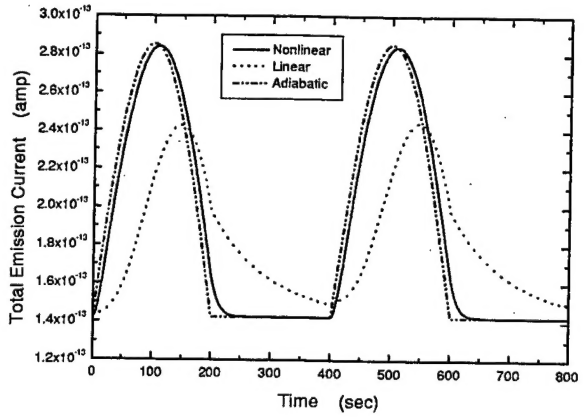

FIG. 8. Total nonadiabatic photoemission current $I_e[\mathcal{E}_b(t), \Phi_{op}(t)] - \Delta I_e(t)$ from the nonlinear and linear models as a function of time for $\mathcal{E}_b(t)=\mathcal{E}_0$. The adiabatic photoemission current $I_e[\mathcal{E}_b, \Phi_{op}(t)]$ with $\mathcal{E}_b(t)=\mathcal{E}_0$ (dash-dot-dotted curve) is also included in the figure for the comparison.

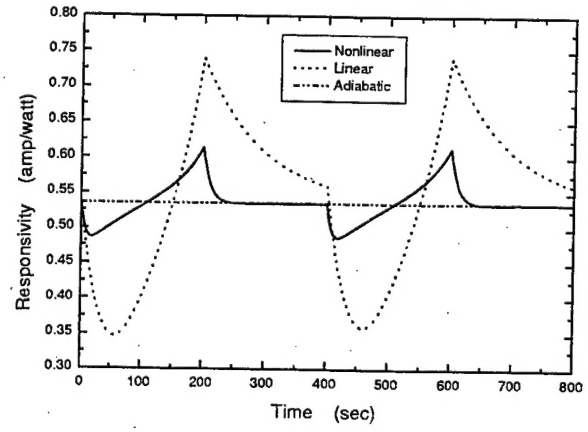

FIG. 9. Dynamical photoresponsivity $\mathcal{R}_{ph}(t)$ from the nonlinear and linear models as a function of time for $\mathcal{E}_b(t)=\mathcal{E}_0$. For convenience, the static photoresponsivity $\mathcal{R}^0_{ph}$ with $\mathcal{E}_b(t)=\mathcal{E}_0$ (dash-dot-dotted line) is also included in the figure.

largevalue of $\Delta I_e(t)$ in the linear model, it is dramatically suppressed by the nonlinearity. This results in the time-dependent photoresponsivity $\mathcal{R}_{ph}(t)$ (solid curve) approaching its static value $\mathcal{R}^0_{ph}$ (dash-dot-dotted line), as can be seen from Fig. 9. From Fig. 9 we also see that the dynamical change of $\mathcal{R}_{ph}(t)$ compared with $\mathcal{R}^0_{ph}$ has been greatly suppressed by the nonlinearity from 40% to 10%. Moreover, the discharging process is finished with a much higher rate due to $C_{QW}[\mathcal{E}_{na}(t)]<C_{QW}[0]$.

IV. CONCLUSIONS AND REMARKS

In conclusion, by deriving the general dynamical equation for $\mathcal{E}_{na}(t)$ in Eqs. (23) and (24) in the presence of both a time-dependent electric field $\mathcal{E}_b(t)$ and a time-dependent incident optical flux $\Phi_{op}(t)$ which provides dual tunneling and photon-assisted escape channels to the system, we have found a compensation of the CF in quantum wells when $\mathcal{E}_b(t)$ and $\Phi_{op}(t)$ become out-of-phase with each other. By working beyond the linear model in Eq. (20), we have found from a nonlinear model in Eq. (19) a large suppression of the nonadiabatic deviation of the photoresponsivity and a speed-up of the discharging process due to the depletion of charge in the quantum wells. For a special case with a dc bias voltage and a time-dependent incident optical flux, the experimentally observed drop of the photoresponsivity as a function of the chopping frequency has been reproduced successfully by our theory. The compensation of the CF in quantum wells predicted in this article will be verified by a future experiment.

ACKNOWLEDGMENTS

The authors gratefully acknowledge many helpful discussions with D. C. Arrington and J. E. Hubbs and some of their data before publication.

[1] A. Singh and D. A. Cardimona, Opt. Eng. **38**, 1424 (1999).
[2] D. H. Huang, A. Singh, and D. A. Cardimona, J. Appl. Phys. **87**, 2427 (2000).
[3] D. C. Arrington, J. E. Hubbs, M. E. Grammer, G. A. Dole, and A. Singh, Proceedings of the Sixth International Symposium on Long Wavelength Infrared Detectors and Arrays: Physics and Applications, edited by S. S. Li, H. C. Liu, M. Z. Tidrow, and S. D. Gunapala, (1999) Vol. 98-21, pp. 29–48; J. E. Hubbs, D. C. Arrington, M. E. Grammer, and G. A. Dole, Opt. Eng. **39**, 2660 (2000).
[4] B. F. Levine, J. Appl. Phys. **74**, R1 (1993).
[5] P. Denk, M. Hartung, M. Streibl, A. Wixforth, K. L. Campman, and A. C. Gossard, Phys. Rev. B **57**, 13094 (1998).
[6] David M.-T. Kuo and Y.-C. Chang, Phys. Rev. B **60**, 15957 (1999).
[7] D. Huang and M. O. Manasreh, Phys. Rev. B **54**, 5620 (1996).
[8] L. El Mir and J. C. Bourgoin, Phys. Status Solidi B **207**, 577 (1998).